# Supporting Information

## SrTiO₃@NiFe LDH core-shell composites for photocatalytic CO₂ conversion

Lian Zhu [a] and Zhengping Qiao*[b]

a. School of Chemistry, Sun Yat-Sen University, Guangzhou, China.

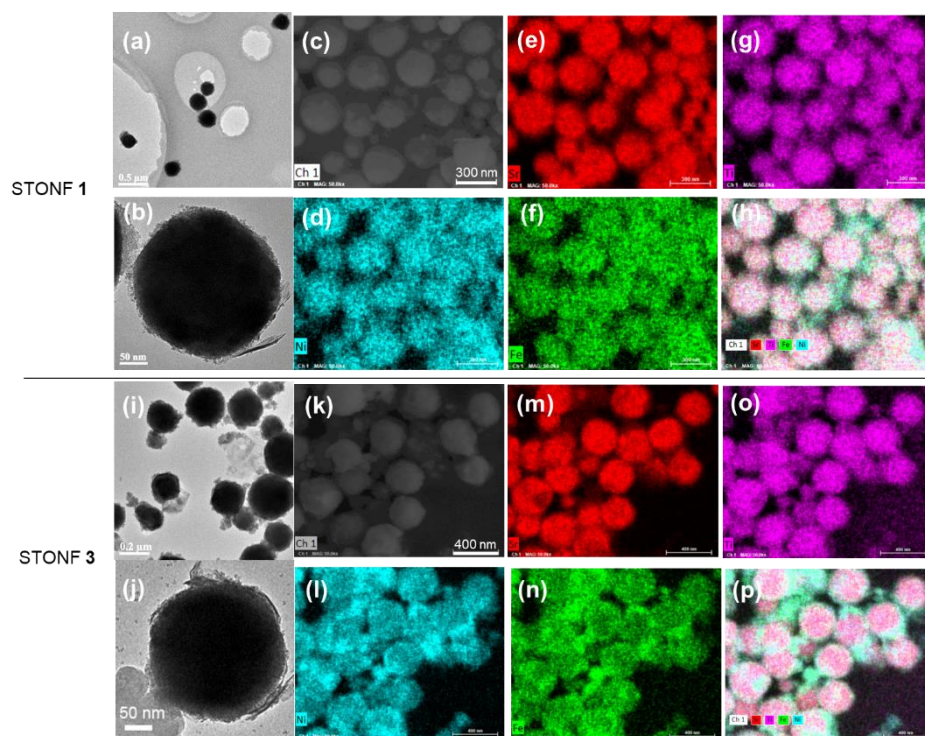b. School of Materials Science and Engineering, Sun Yat-Sen University, Guangzhou, China.

Fig. S1 (a-b) TEM image of STONF **1**; (c-h) EDS element mappings of STONF **1**; (i-j) TEM of STONF **3**; (k-p) EDS element mappings of STONF **3**. Magnification and scale bar of (d-h) and (l-p) is identical to that of (c) and (k) respectively.

Table S1 Summary of CO$_2$ reduction performance of SrTiO$_3$-based and LDH-based photocatalysts.

| Catalysts | Condition | Performance | Reference |
|---|---|---|---|
| SrTiO$_3$ nanorod thin film | 0.5 M KHCO$_3$ electrolyte solution Hg–Xe lamp | < 0.2 µmol g$^{-1}$ CO (in 5 h) | 1 |
| Al-SrTiO$_3$/Ag | 0.1 M NaHCO$_3$ aqueous 400 W Hg lamp, λ > 300 nm 0.5 g catalysts | 2.6 µmol h$^{-1}$ CO CH$_4$ | 2 |
| Ag/SrTiO$_3$ | 0.1 M NaHCO$_3$ 400 W Hg lamp, λ > 300 nm 0.5 g catalysts | < 0.4 µmol h$^{-1}$ CO | 3 |
| 5:1-NiFe LDH | H$_2$O, TEOA 300 W Xe lamp | ~ 4 µmol g$^{-1}$ h$^{-1}$ CO ~ 0.8 µmol g$^{-1}$ h$^{-1}$ CH$_4$ (in 3h) | 4 |
| NiFe-LDH/Cu$_2$O | NaHCO$_3$ and H$_2$SO$_4$ react to produce CO$_2$ 300 W Xe lamp, λ > 420 nm | < 0.5 µmol g$^{-1}$ h$^{-1}$ CO (in 3h) | 5 |
| MgAl LDH | H$_2$O 300 W Xe lamp | 0.1 µmol g$^{-1}$ CO (in 3 h) | 6 |
| Co-porphyrin/ MgAl LDH | H$_2$O 300 W Xe lamp | 0.4 µmol g$^{-1}$ h$^{-1}$ CO 0.24 µmol g$^{-1}$ h$^{-1}$ CH$_4$ | 6 |
| Pt/MgAl LDH | H$_2$O 300 W Xe lamp | 2.64 µmol g$^{-1}$ h$^{-1}$ CO | 7 |
| CoMgAl LDH | CH$_3$CN/TEOA 300 W Xe lamp, λ > 400 nm | ~0 µmol h$^{-1}$ CO | 8 |
| CoAl-LDH@TiO$_2$ | H$_2$O 300 W Xe lamp | 4.57 µmol g$^{-1}$ h$^{-1}$ CO 0.41 µmol g$^{-1}$ h$^{-1}$ CH$_4$ | 9 |
| CoAl-LDH/TiO$_2$ | H$_2$O 300 W Xe lamp | < 2.5 µmol g$^{-1}$ h$^{-1}$ CO ~0.3 µmol g$^{-1}$ h$^{-1}$ H$_2$ < 1.2 µmol g$^{-1}$ h$^{-1}$ O$_2$ | 10 |

| | | | |
|---|---|---|---|
| g-C$_3$N$_4$/NiAl-LDH | H$_2$O<br>300 W Xe lamp<br>λ > 420 nm | 1.5 μmol g$^{-1}$ CO<br>(in 3 h) | 11 |
| Bi$_2$O$_2$CO$_3$/Bi/NiAl-LDH | H$_2$O<br>300 W Xe lamp<br>λ < 800 nm | < 2 μmol g$^{-1}$ h$^{-1}$ CO<br>~10 μmol g$^{-1}$ h$^{-1}$<br>CH$_4$ | 12 |
| Ti$_3$C$_2$T$_x$ MXene/NiAl LDH | CH$_3$CN, H$_2$O, TEOA<br>300 W Xe lamp | ~0 μmol g$^{-1}$ h$^{-1}$ CO | 13 |
| Pt/ZnCr LDH | 200 W Hg–Xe lamps<br>UV irradiation | < 8 μmol g$^{-1}$ CO<br>(in 3 h) | 14 |
| Pd/ZnCr LDH | 200 W Hg–Xe lamps<br>UV irradiation | ~5 μmol g$^{-1}$ CO<br>(in 3 h) | 14 |
| Au/ZnCr LDH | 200 W Hg–Xe lamps<br>UV irradiation | ~3 μmol g$^{-1}$ CO<br>(in 3 h) | 14 |
| SrTiO$_3$/NiFe LDH | H$_2$O<br>300 W Xe lamp | 4.6 μmol g$^{-1}$ h$^{-1}$ CO<br>2.8 μmol g$^{-1}$ h$^{-1}$ CH$_4$<br>(in 3 h) | this work |
| SrTiO$_3$/NiFe LDH | CH$_3$CN/TEOA<br>300 W Xe lamp | 7.9 μmol g$^{-1}$ h$^{-1}$ CO<br>1.5 μmol g$^{-1}$ h$^{-1}$ CH$_4$<br>(in 3 h) | this work |

(a)

¹H NMR (400 MHz, D₂O)

δ 4.69, 4.14, 4.13, 4.12, 3.21, 3.19, 3.18, 2.58.

before photocatalysis

(b) ¹H NMR (400 MHz, D₂O)

δ 4.69, 4.17, 4.16, 4.15, 3.25, 3.24, 3.22, 2.59.
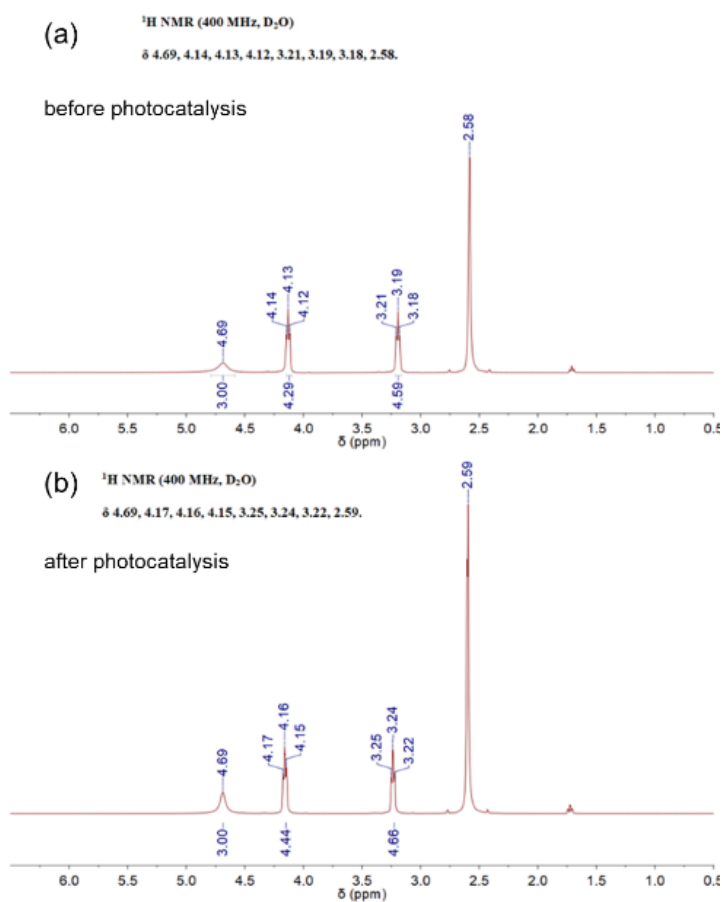
after photocatalysis

Fig. S2 ¹H NMR of reaction mixture before (a) and after photocatalysis (b).

¹H NMR spectrum of reaction mixture before photocatalysis was the same as the one after photocatalysis. Peaks at 2.58 ppm can be assigned to acetonitrile. Peaks around 4.69, 4.16 and 3.24 ppm can be assigned to TEOA. So $CH_4$, CO and probable liquid products were not detected, including HCHO, $CH_3OH$, HCOOH, $CH_3CHO$, and $CH_3COOH$.
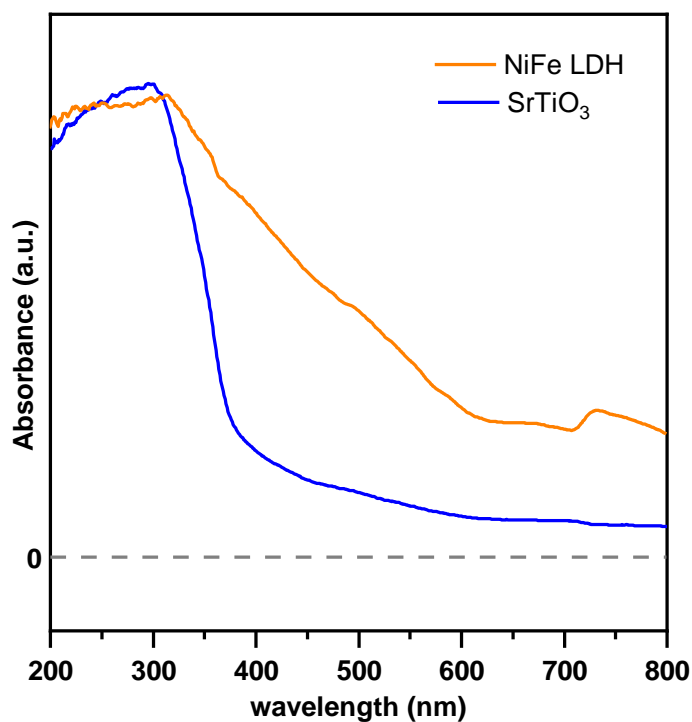
Fig. S3 Absorption spectrum of SrTiO₃ and NiFe LDH

As showed in Fig. S3, bare SrTiO$_3$ showed absorption edge at 380 nm, arising from the wide bandgap. Meanwhile, it showed weak absorption in visible light region, which attributed to the defective of SrTiO$_3$. References (Ref. 20-24 in manuscript) also reported that SrTiO$_3$ showed weak visible light and even infrared absorption and its visible light photocatalytic activity, including water splitting, tetracycline degradation, dye degradation and NO decomposition.
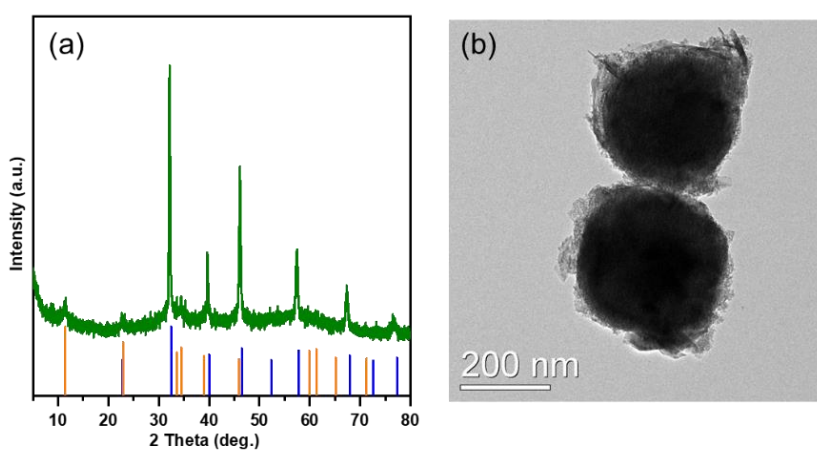


Fig. S4 PXRD (a) and TEM image (b) of STONF **2** after 5 catalysis cycles. (orange line: NiFe LDH standard patterns, blue line: SrTiO$_3$ standard patterns, green line: STONF **2**)

**Determination of band structure:**

In Mott-Schottky graph, the slope of linear segment represents the semiconductor type. The n-type semiconductor shows positive slope and reversely p-type semiconductor shows negative slope. As shown in Fig. 4b, as-prepared $SrTiO_3$ and NiFe LDH were both n-type. Generally, for n-type semiconductor, flat band potential ($E_f$) approximately equals to potential of conduction band bottom (ECB). Therefore, the ECB of $SrTiO_3$ and NiFe LDH was −0.75 V and −0.87 V (vs. NHE), respectively. The potential of valence band top (EVB) can be calculated by adding $E_g$ and ECB values. As a result, EVB of $SrTiO_3$ was 2.35 V (−0.75+3.1=2.35). EVB of NiFe LDH was 1.33 V (−0.87+2.2=1.33).

Table S2 Fitting parameters of transient PL decays of as-prepared catalysts.

| | $\tau_1$ (ns) | | $\tau_2$ (ns) | | $\tau_3$ (ns) | | $\tau$ (ns) |
|---|---|---|---|---|---|---|---|
| | lifetime | R% | lifetime | R% | lifetime | R% | |
| STONF **1** | 1.26 | 64.2% | 6.66 | 35.8% | - | - | 3.19 |
| STONF **2** | 0.56 | 24.9% | 5.96 | 71.2% | 16.65 | 3.9% | 5.03 |
| STONF **3** | 1.25 | 69.3% | 6.38 | 30.7% | - | - | 2.82 |

Fitting parameters of Nyquist plots was shown in Table S3. $R_s$ and $R_w$ referred to solution resistance and diffusion resistance, which were not involved in photocatalysis.

Table S3 Fitting parameters of Nyquist plots

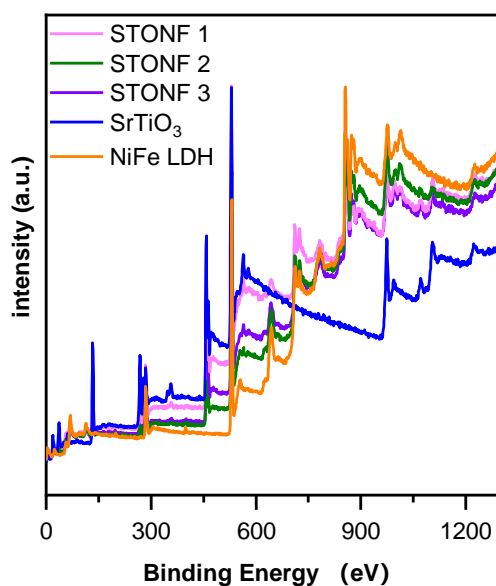| Substance | $R_s$ ($\Omega$ cm$^{-2}$) | $R_{ct}$ ($\Omega$ cm$^{-2}$) | $R_w$ ($10^{-3}\Omega$ cm$^{-2}$) |
|---|---|---|---|
| $SrTiO_3$ | 14.8 | 10.22 | 1.359 |
| NiFe LDH | 11.75 | 25.4 | 1.342 |
| STONF **1** | 13.21 | 15.38 | 1.25 |
| STONF **2** | 14.11 | 13.08 | 1.249 |
| STONF **3** | 12.97 | 16.06 | 1.308 |

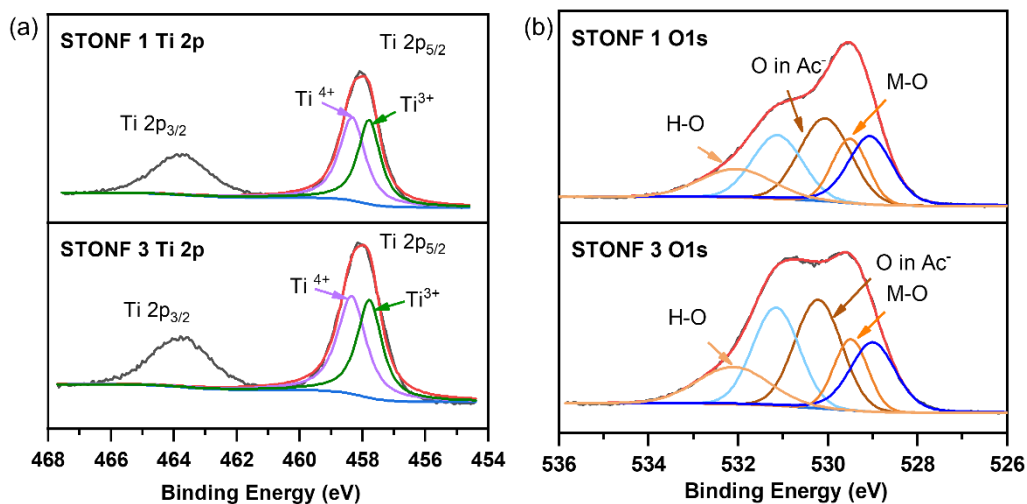Fig. S5 XPS survey of NiFe LDH, SrTiO$_3$ and STONF **2**.



Fig. S6 XPS spectra of (a) the Ti 2p region and (b) O 1s region for STONF **1** and **3**.

$R_1$ and $R_2$ value was 1~3>2 and 3>1>2, respectively. This indicated $V_o$ concentration was 3>1>2. The sequence was in accordance with photocatalytic performance.

**References**

1. S. Shoji, G. Yin, M. Nishikawa, D. Atarashi, E. Sakai and M. Miyauchi, *Chem. Phys. Lett.*, 2016, **658**, 309-314.
2. S. Wang, K. Teramura, T. Hisatomi, K. Domen, H. Asakura, S. Hosokawa and T. Tanaka, *ACS Sustainable Chem. Eng.*, 2021, **9**, 9327-9335.
3. S. Wang, K. Teramura, T. Hisatomi, K. Domen, H. Asakura, S. Hosokawa and T. Tanaka, *ACS Appl. Energy Mater.*, 2020, **3**, 1468-1475.
4. X. Zhao, X. Zhao, I. Ullah, L. Gao, J. Zhang and J. Lu, *Catal. Lett.*, 2021, **151**, 1683-1692.
5. Y. Wu, Y. Gong, J. Liu, T. Chen, Q. Liu, Y. Zhu, L. Niu, C. Li, X. Liu, C. Q. Sun and S. Xu, *J. Alloys Compd.*, 2020, **831**, 154723.
6. J. Xu, X. Liu, Z. Zhou, L. Deng, L. Liu and M. Xu, *Energy Fuels*, 2021, **35**, 16134-16143.
7. J. Xu, X. Liu, Z. Zhou, L. Deng, L. Liu and M. Xu, *Energy Fuels*, 2021, **35**, 10820-10831.
8. C. Ning, Z. Wang, S. Bai, L. Tan, H. Dong, Y. Xu, X. Hao, T. Shen, J. Zhao, P. Zhao, Z. Li, Y. Zhao and Y.-F. Song, *Chem. Eng. J.*, 2021, **412**, 128362.
9. S. Kumar, L. J. Durndell, J. C. Manayil, M. A. Isaacs, C. M. A. Parlett, S. Karthikeyan, R. E. Douthwaite, B. Coulson, K. Wilson and A. F. Lee, *Part. Part. Syst. Charact.*, 2018, **35**, 1700317.
10. S. Kumar, M. A. Isaacs, R. Trofimovaite, L. Durndell, C. M. A. Parlett, R. E. Douthwaite, B. Coulson, M. C. R. Cockett, K. Wilson and A. F. Lee, Appl. Catal. B, 2017, **209**, 394-404.
11. S. Tonda, S. Kumar, M. Bhardwaj, P. Yadav and S. Ogale, *ACS Appl. Mater. Interfaces*, 2018, **10**, 2667-2678.
12. Y.-f. Miao, R.-t. Guo, J.-w. Gu, Y.-z. Liu, G.-l. Wu, C.-p. Duan and W.-g. Pan, *ACS Appl. Nano Mater.*, 2021, **4**, 4902-4911.
13. S. Zhao, D. Pan, Q. Liang, M. Zhou, C. Yao, S. Xu and Z. Li, *J. Phys. Chem. C*, 2021, **125**, 10207-10218.
14. K.-i. Katsumata, K. Sakai, K. Ikeda, G. Carja, N. Matsushita and K. Okada, *Mater. Lett.*, 2013, **107**, 138-140.